HHS Public Access

Author manuscript

Cell Rep. Author manuscript; available in PMC 2017 August 10.

Published in final edited form as:

Cell Rep. 2017 June 27; 19(13): 2853–2866. doi:10.1016/j.celrep.2017.06.016.

An Integrative Framework Reveals Signaling-to-Transcription Events in Toll-Like Receptor Signaling

Philipp Mertins[1,8], **Dariusz Przybylski**[1,8], **Nir Yosef**[1,2], **Jana Qiao**[1], **Karl Clauser**[1], **Raktima Raychowdhury**[1], **Thomas M. Eisenhaure**[1], **Tanja Maritzen**[3], **Volker Haucke**[3], **Takashi Satoh**[4], **Shizuo Akira**[4], **Steven A. Carr**[1], **Aviv Regev**[1,5,*], **Nir Hacohen**[1,6,*], and **Nicolas Chevrier**[1,7,9,*]

[1]Broad Institute of MIT and Harvard, 7 Cambridge Center, Cambridge, MA 02142, USA

[2]Department of Electrical Engineering and Computer Science and Center for Computational Biology, University of California, Berkeley, Berkeley, CA 94720, USA

[3]Molecular Physiology and Cell Biology Section, Leibniz-Institute for Molecular Pharmacology (FMP), Berlin, Germany

[4]WPI Immunology Frontier Research Center, Osaka University, 3-1 Yamada-oka, Suita, Osaka 565-0871, Japan

[5]Howard Hughes Medical Institute, Department of Biology, MIT, Cambridge, MA 02142, USA

[6]Center for Immunology and Inflammatory Diseases and Center for Cancer Research, Massachusetts General Hospital, Charlestown, MA 02129, USA

Summary

Building an integrated view of cellular responses to environmental cues remains a fundamental challenge due to the complexity of intracellular networks in mammalian cells. Here we introduce an integrative biochemical and genetic framework to dissect signal transduction events using multiple data types, and in particular, to unify signaling and transcriptional networks. Using the Toll-like receptor (TLR) system as a model cellular response, we generate comprehensive datasets of physical, enzymatic, and functional interactions, and integrate these data to reveal biochemical paths that connect TLR4 signaling to transcription. We define the roles of proximal TLR4 kinases,

*Correspondence: aregev@broadinstitute.org (A.R.), nhacohen@mgh.harvard.edu (N.H.), chevrier@fas.harvard.edu (N.C.).
[7]Present address: FAS Center for Systems Biology, Harvard University, Cambridge, MA 02138, USA
[8]These authors contributed equally
[9]Lead contact

ACCESSION NUMBERS

The original mass spectra may be downloaded from MassIVE (http://massive.ucsd.edu) using the identifier: MSV000081071. The data is directly accessible via ftp://massive.ucsd.edu/MSV000081071.

AUTHOR CONTRIBUTIONS

N.C. designed study and performed experiments; P.M. and J.Q. performed mass spectrometry; R.R. and T.M.E. contributed to experiments; D.P., P.M., N.Y. and N.C. performed computational analyses; T.M., V.H., T.S., and S.A. contributed knockout bone marrow cells; P.M., D.P., S.A.C., A.R., N.H. and N.C. wrote the manuscript with input from all authors. This work was supported by NIH grant U54 AI057159, the NIH New Innovator Award DP2 OD002230 (N.H.), NIH P50 HG006193 (A.R., N.H.), and the Bauer Fellows Program (N.C.).

identify and functionally test two dozen candidate regulators, and demonstrate a role for *Ap1ar* (encoding the Gadkin protein) and its binding partner *Picalm*, potentially linking vesicle transport with pro-inflammatory responses. Our study thus demonstrates how deciphering dynamic cellular responses by integrating datasets on various regulatory layers defines key components and higher-order logic underlying signaling-to-transcription pathways.

Graphical Abstract

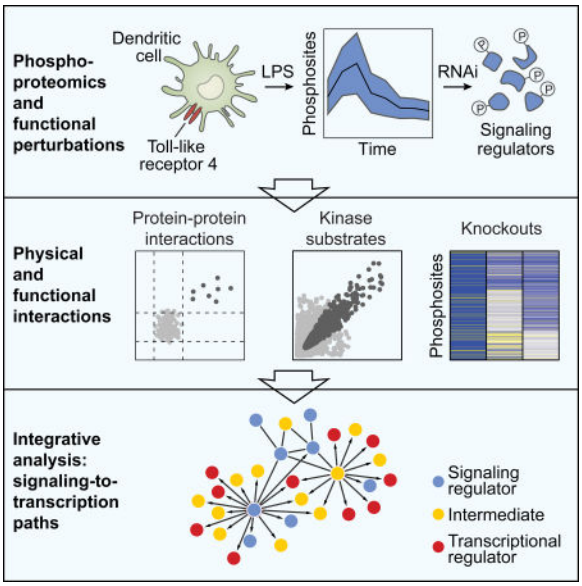

Introduction

Signaling networks must coordinate multiple layers of regulation throughout the cell to respond to environmental changes. For example, mammalian immune cells detect microbial molecules thanks to pathogen-sensing pathways such as Toll-like receptors (TLRs) (Takeuchi and Akira, 2010). Upon activation by their cognate ligands, TLRs follow general principles of signal transduction by recruiting cytosolic adaptors and downstream enzymes such as kinases, which triggers cascades of biochemical changes leading to cellular outputs such as gene expression changes (Figure 1A and 1B). A fundamental question in cellular response systems, such as TLRs, is how to generate and combine knowledge about signaling and transcription regulatory networks to build an integrated view of the flow of information in a cell. Answering this question will help close gaps in our knowledge of intracellular wiring and inform therapeutic targeting of cellular components that are central to disease.

Despite recent advances in measuring cellular processes and associated biochemical changes from many different angles (*e.g.*, post-translational modifications, gene expression, transcription factor binding), building integrated models of signaling pathways that take into account multiple regulatory layers remains an elusive task due to several challenges. First, using prior knowledge from databases alone, it is hard to compare and connect signaling nodes and processes that have been studied in disparate systems and with different readouts. Furthermore, existing databases are largely incomplete, as demonstrated by the fact that the

vast majority of known phosphorylation sites remain orphans with respect to their matching kinases. Second, acquiring data within a single cellular context and across regulatory processes ranging from post-translational modifications (PTMs) to protein complexes to kinase substrates is difficult due to the various technical requirements of each assay, making them hard to adapt within a unique and relevant cellular context. Third, individual large-scale measurements are inherently limited by their variability in sensitivity and specificity, and are often used to capture static snapshots rather than the dynamic events of cellular responses. It is thus critical to address these challenges to help to dissect the connections that form the basis of multi-layered cellular responses (Bensimon et al., 2012; Santra et al., 2014; Yugi et al., 2016).

Here we hypothesized that integrating measurements spanning, in the context of a single cellular response model, both signaling and transcriptional regulatory layers will help to reveal key network-wide properties that would otherwise not be observable. To test this, building upon prior work (Chevrier et al., 2011), we developed an experimental and computational framework to measure and integrate the information underlying signaling-to-transcription events in the TLR system – from the membrane to gene regulation. We measure dynamic changes in two types of interactions: physical (*i.e.*, phosphorylation, kinase-substrate relationships, protein-protein and DNA-protein interactions), and functional (*i.e.*, effects of genetic perturbations on gene expression or phosphorylation events) (Figure S1A). Using these data sets, we identify regulators of TLR4 responses in dendritic cells (DCs), including AP1AR and its binding partner PICALM, and introduce a network-based computational approach that takes advantage of these diverse measurements to decipher the higher-order logic governing TLR signaling-to-transcription events.

Results

The dynamic phosphoproteome of LPS-stimulated dendritic cells

We reasoned that large-scale, dynamic measurements of the changes in protein phosphorylation in lipopolysaccharide (LPS)-treated DCs would help to reconstruct signaling-to-transcription pathways because TLR signaling functions through phosphorylation of its own constituents – from kinases such as MAP kinases, IRAKs, IKKs or TBK1, to transcription factors such as NF-κB or IRFs (Figure 1B) (Takeuchi and Akira, 2010). Furthermore, work by others (Sharma et al., 2010; Sjoelund et al., 2014; Weintz et al., 2010) and us (Chevrier et al., 2011) showed that phosphoproteomics can identify regulators of the TLR system. We used SILAC-based phosphoproteomics to compare the levels of phospho-serine, -threonine, and -tyrosine sites between DCs left untreated as control or stimulated with LPS at 8 time points (15, 30, 45, 60, 120, 180, 240 and 360 minutes) (Figure S1B and S1C). We identified and quantified a total of 20,975 phosphosites derived from 5,789 distinct proteins in at least two LPS-stimulated samples (FDR < 1%; Figure 1C and Table S1), of which 20.5% were present in all 8 time points (4,310/20,975 phosphosites from 1,952 proteins; Figure S1D) due to undersampling of highly complex and low signal intensity phosphopeptides mixtures in individual SILAC experiments. The largest changes in the DC phosphoproteome were observed at 30 and 45 min after LPS stimulation, which covered 92.8% of all quantified phosphosites in this study (19,456/20,795) (Figure

S1E). In addition, these changes in phosphorylation were not due to changes in protein amounts: only 0.65 and 1.81% of proteins showed an increase in both phosphorylation and protein levels at 2 and 6 h after LPS stimulation, respectively (Figure 1D). These results suggested that LPS stimulation modifies a large fraction of the DC phosphoproteome within an hour.

Temporal analysis of phosphorylation changes highlights known and candidate regulators of TLR4 signaling

Next, to study the dynamics of the LPS-regulated phosphoproteome, we focused on the 3,557 phosphosites mapping onto 1,606 proteins that were quantified in at least 6 out of 8 time points, and differentially regulated upon LPS stimulation in a single or two consecutive time points (2,071/3,557 phosphosites for the latter) (Table S2). Overall, 53.4% (3,557/6,659) of the phosphosites quantified in at least 6 independent time points were found to be differentially regulated by LPS, which corresponds to 61.4% (1,606/2,617) at the phosphoprotein level. We used *k*-means clustering to partition these 3,557 phosphosites into 10 co-abundance clusters with distinct temporal profiles (Figure 2A and S2A). We found three general patterns of changes in phosphorylation levels: (1) early upregulation until 45 min (clusters I and II), (2) late upregulation after 120 min (cluster III), and (3) downregulation at various times (clusters IV through X) (Figure 2B). Each temporal cluster contained known TLR pathway proteins for a total of 43 out of 141 canonical TLR components, including 7.8% (11/141) and 10.6% (15/141) for clusters I and II, respectively (Figure 2B and Figure S2B). Known TLR proteins identified in this data encompassed both positive (*e.g.*, MAPK family, IRF3, NF-κB) and negative (*e.g.*, TANK, TNFAIP3) regulators, and were differentially phosphorylated at multiple sites in some cases (Figure S2C). The 1,606 phosphoproteins present in these 10 temporal clusters were enriched for molecular functions including kinases, transcriptional regulators, or protein binding (Figure S2D). Some of the enriched gene sets pointed to nascent areas of TLR biology, such as the organization and regulation of the TLR system within the framework of intracellular organelles and structures (*e.g.*, activity and regulation of GTPases, cytoskeleton; Figure S2D). Cluster II, and to a lesser extent other clusters, showed a significant enrichment for other immune signaling pathways (*e.g.*, B and T cell receptor signaling, or DNA sensing pathways), highlighting the existence of shared proteins between these immune response systems (Figure S2D). Taken together, these results reveal the dynamic changes imparted on the DC phosphoproteome by LPS, which include known and putative regulators of TLR4 signaling as well as processes linked to DC biology such as changes in cell shape, motility, metabolism and antigen processing.

Genetic perturbations of phosphorylated proteins identify putative regulators of TLR4 signaling

To test if the phosphoproteins identified above play a role in the TLR system, we used our temporal and enrichment analyses to prioritize candidates for genetic perturbations (Figure 3A). We focused on 751 phosphoproteins from the 1,606 ones used for temporal clustering, which were upregulated at 30 and 45 min after LPS (clusters I and II; Figure 2B). We reasoned that using early clusters would help to identify candidate regulators likely to be downstream of TLR4 by avoiding feedbacks from transcription or autocrine and paracrine

signaling. Third, we selected 168/751 phosphoproteins to test by retaining all enzymes (*e.g.*, kinases, GTPases) and enzyme binders and regulators (*e.g.*, GTPase regulators) (Figure S3A, S3B and Table S3). All selected phosphoproteins where also found to be expressed at the mRNA level in DCs (Garber et al., 2012). The two TLR4 adaptor proteins MYD88 and TRIF (encoded by *Ticam1*) were part of these 131 genes. MYD88 was added manually as a positive control, although it was not found to be differentially phosphorylated, whereas TRIF matched our selection criteria above.

We successfully perturbed 131 out of 168 candidate genes with an average knockdown efficiency of 81 +/− 9% S.D. (Figure S3C). We stimulated DCs with LPS and measured the effect of gene silencing on the mRNA levels of 263 TLR response signature genes, representing the inflammatory and antiviral programs (Table S3). We determined statistically significant changes in the expression of signature transcripts upon individual knockdowns based on comparisons to 16 control genes, whose expression remains unchanged upon TLR activation, and to 38 control shRNAs that did not affect TLR signature genes. 27 out of the 131 genes tested significantly affected TLR signature gene expression, which included known TLR signaling components such as TICAM1, TBK1, MAPK9, RIPK3 and IRAK2 (Figure 3B). Furthermore, several phosphoproteins were reported to function in TLR signaling by independent studies: TRAFD1 (Sanada et al., 2008), STK3 (Geng et al., 2015), ULK1 (Eriksen et al., 2015), and CORO1A (Tanigawa et al., 2009). Interestingly, known and candidate components had similar effects on the TLR gene signature upon knockdown. By measuring the pairwise similarity among these 27 perturbation profiles (using Pearson's correlation), we observed three major modules of signaling regulators: MYD88 and a set of 4 proteins (SAMHD1, TBC1D17, AP1AR, and PDLIM7) affecting inflammatory gene expression (module I), TICAM1 and 5 proteins (module II), and 16 proteins displaying effects that overlap with MYD88 and/or TICAM1 (module III) (Figure 3B).

Validation of AP1AR and other candidate regulators of the Myd88-dependent inflammatory pathway

We next sought to validate the putative roles of the 4 phosphoproteins – AP1AR, PDLIM7, SAMHD1, and TBC1D17 – whose perturbation profiles closely resembled that of MYD88 in controlling pro-inflammatory genes (Figure 4A). We measured the expression levels of inflammatory and antiviral cytokines in LPS-stimulated DCs infected by 2 independent, gene-specific lentiviral shRNAs per candidate phosphoprotein. We observed a decrease in inflammatory cytokine mRNA expression compared to 8 control hairpins in all cases (*Il6*, *Cxcl1*, and to a lesser extent for *Tnf*), whereas antiviral cytokines Ifit1 and Cxcl10 were mostly unaffected (Figure 4B). Similarly, using mouse *Ap1ar*$^{-/-}$ knockout DCs (Maritzen et al., 2012), we observed a strong decrease in inflammatory cytokines, especially *Il1b*, *Il12b*, and *Tnf*, whereas antiviral cytokines were not affected (*Ifnb1*) or slightly reduced (*Cxcl10*) (Figure 4C).

To generate mechanistic insights about the putative role of AP1AR in the TLR4 pathway, we sought to identify binding partners of AP1AR in LPS-stimulated DCs using affinity purification followed by mass spectrometry in primary mouse DCs (Figure S4A). Protein overexpression was effective in nearly all transduced cells as measured by GFP

fluorescence, and did not impact cell responsiveness to LPS as shown by strong morphological changes (Figure S4B). We overexpressed V5-tagged AP1AR and GFP as control bait in SILAC labeled DCs stimulated with LPS for 30 min (Figure S4C), which led to the identification of proteins that co-precipitated with AP1AR, but not GFP (Figure 4D and Table S4). Several known components of the assembly protein complex 2 (AP-2) were pulled down with AP1AR (AP2A1, AP2B1, AP2S1), as well as the AP-2 binding partner PICALM which is an important component of clathrin mediated endocytosis (Miller et al., 2015). Next, to test if some of these AP1AR binders affect TLR4 signaling outputs, we turned back to genetic perturbations followed by gene signature measurements. Out of 10 putative AP1AR binders (at least 2 peptides identified and >1.5 log2 SILAC ratio of AP1AR/GFP), 6 showed a knockdown efficiency > 50%. We found that PICALM led to a decrease in the induction of LPS-induced inflammatory genes similarly to MYD88, TIRAP and AP1AR (Figure 4E). Altogether, these results suggest a potential mechanism whereby AP1AR and PICALM act together in the regulation of MYD88-dependent inflammatory signaling.

For another candidate identified based on phosphorylation changes – SAMHD1 – we further tested its potential involvement in TLR signaling using human skin fibroblasts derived from Aicardi-Goutières syndrome (AGS) patients that carry deleterious SAMHD1 mutations (Crow and Manel, 2015). We observed a decrease in both inflammatory and antiviral gene expression upon LPS stimulation in 2 independent patient cell lines compared to 3 healthy controls (Figure 4F), which differed from knockout mouse DC data (Figure S4D). The latter observation might be attributable to the difference in cellular context or to compensatory mechanisms in the mouse knockout cells. Interestingly, physical interactions between SAMHD1 and TLR pathway proteins have been reported previously, such as the TLR4 adaptor protein TIRAP (Li et al., 2011) and also with CCNA2 and CDK2 that can be activated by TLR4 signaling (Hasan et al., 2007; Huttlin et al., 2015). Altogether, we gathered evidence supporting that AP1AR, its binding partner PICALM, and SAMHD1 are likely to act as regulators of pro-inflammatory TLR4 signaling.

Signaling regulator perturbation profiles overlap with transcription factor target genes, suggesting potential signaling-to-transcription paths

Having shown that phosphorylation dynamics can help identify potential regulators of TLR signaling-to-transcription events, we next sought to identify how signaling regulators are connected to downstream transcriptional regulators. The two targeted screens for candidate (i) phosphoproteins and (ii) AP1AR binders led to 29 perturbation profiles showing significant changes in TLR signature genes upon LPS stimulation (Figure 3B and 4E). Based on the similarity of these perturbation-induced expression profiles (Pearson’s correlation), we partitioned these 29 proteins into 3 modules (Figure 5A; similar to Figure 3B). Next, we asked what transcription factors (TFs) are likely to act downstream of these 3 modules of proteins by taking advantage of existing data on the binding sites across the genome of 23 TFs involved in TLR4 signaling (Garber et al., 2012). We reasoned that measuring the overlaps between genes whose promoters are bound by a TF, and genes whose mRNA levels are impacted by knockdown of a phosphoprotein, would help to infer some of the signaling regulator-TF relationships likely to be active upon TLR4 activation (Figure S5). For 20 out

of 23 TFs tested, we identified significant overlaps (p-value < 0.05; hypergeometric test) between gene sets whose promoters were bound by one or several TFs, and those whose mRNA levels were impacted by knockdown of 25/29 candidate and known regulators (Figure 5B and Table S5). Some of these overlaps recapitulated known signaling regulator-TF relationships in the TLR pathways, such as MYD88 and NF-κB family members REL and RELB, or TRIF and IRFs and STATs. Gene targets of AP1AR, MYD88 and PICALM overlapped significantly with genes bound by RUNX1 and REL. Taken together, these results further support a role for the 29 phosphoproteins identified here downstream of TLR4 by, and suggest signaling regulator-TF relationships between 25 phosphoproteins and 20 TFs.

Physical and functional proteomics pinpoint binding and phosphorylation events downstream of the Myd88 adaptor and associate kinases

Next, to decipher the biochemical events linking the signaling to transcriptional regulator relationships identified above, we measured protein-protein and kinase-substrate interactions by focusing on MYD88-dependent signaling. First, in DCs stimulated with LPS for 30 min, we rediscovered most known MYD88 binding partners, including TIRAP, TRAF6 or IRAK family kinases, which support the validity of our AP-MS assay in primary DCs (Figure 6A, S6A and Table S6). IRAK2 immunoprecipitation identified several interaction partners such as MYD88 and TRAF6 but with lower enrichment ratios compared to MYD88, which is likely due to the short-lived interaction dynamics of kinases (Figure 6B).

Second, we used two complementary approaches to identify the substrates downstream of MYD88-associated kinases, which remain poorly characterized. Perturbation approaches followed by phosphoproteomics have proven useful in determining functional pathway components downstream of a given network node (Bodenmiller et al., 2010; Chevrier et al., 2011). We measured the impact of 4 knockout (KO) models: *Myd88*$^{-/-}$, *Myd88*$^{-/-}$/*Ticam1*$^{-/-}$ (which abrogates all TLR4 signals), *Irak2*$^{-/-}$ and *Irak4*$^{-/-}$, on the DC phosphoproteome upon LPS stimulation for 30 min (Figure 6C and 6D). To stringently evaluate KO effects on the LPS-dependent DC phosphoproteome, we focused on the 1628 phosphosites mapping onto 990 unique proteins that were differentially regulated in both (1) LPS-treated wild-type DCs at 30–45 min (time course data; Table S1) and (2) *Myd88*$^{-/-}$/*Ticam1*$^{-/-}$ DCs compared to wild-type (Table S6). Out of these 1628 phosphosites, a third (38.1%, 621/1628) were only affected by *Myd88*$^{-/-}$/*Ticam1*$^{-/-}$ double deletion, whereas the remaining sites were affected by both double and single mutants: 45.6% (742/1628) for *Irak4*$^{-/-}$, 31.1% (506/1628) for *Myd88*$^{-/-}$, and 8.1% (132/1628) for *Irak2*$^{-/-}$. These numbers agree with the essential role of IRAK4 in TLR signaling (Picard et al., 2003; Suzuki et al., 2002), and the partially redundant function of IRAK2 with IRAK1 (Kawagoe et al., 2008). Furthermore, these 990 Myd88/Ticam1-dependent phosphoproteins captured 32.6% (46/141) of the canonical TLR proteins, including known phosphosites such as TBK1 S716 and JUN S63/S73 downregulated in *Myd88*$^{-/-}$ and *Irak4*$^{-/-}$ cells, IRF3 S379 impacted upon double KO only, or MAPK9 T183/Y185 by MYD88- and TRIF-dependent pathways (Figure S6B).

To complement this genetic approach, we developed a large-scale *in vitro* kinase (IVK) assay using recombinant kinases IRAK4, TBK1, and IRAK2 mixed with native protein lysates from SILAC-labeled DCs followed by phosphoproteomics (Figure 6E). We identified a total of 967 phosphosites upregulated by IRAK4, 325 by TBK1, and 201 by IRAK2, which included sites also upregulated in LPS-treated DCs: 55/967 (5.7%) for IRAK4 and 62/325 (19.1%) for TBK1 (Figure 6F, 6G and Figure S6C and Table S6). These results suggest that some of the phosphosites identified by IVK are likely to be physiologically relevant, although others might be due to off targets effects (*e.g.*, activation of secondary kinases, or proximity with proteins in solution that would not exist in cells).

An integrated model reveals signaling-to-transcription paths across the TLR4 system

Lastly, we sought to combine our measurements on physical and functional interactions into an integrated model of signaling-to-transcription relationships in the TLR4 system (Figure S7A). We used a network-based approach that relies on three main steps (Figure 7A). First, we assembled a 'background' network of 92,610 protein-protein and 5,533 kinase-substrate interactions from public repositories, and 43 protein-protein and 230 kinase-substrate interactions identified from this study using DCs (Table S7). Second, we assigned weights to the edges (*i.e.*, protein-protein and kinase-substrate interactions) and nodes (*i.e.*, signaling or transcriptional regulators) of the background network, to create a 'weighted' interaction network based on the phosphorylation changes driven by LPS stimulation and specific kinases (based on KO and IVK data). Third, we searched the weighted network for biochemical paths linking the 29 phosphoproteins or 'seed nodes' to transcriptional regulators or 'target nodes'. To test the validity of this integrative algorithm, we quantified its performance in retrieving known seed-target relationships between canonical TLR pathway components using receiver operator characteristic (ROC) curves. In the high precision regime, using a weighted network outperformed methods that used the background interaction network or phosphorylation data alone. For example, at a false positive rate (FPR) = 0.001, the 'weighted network' method yielded a true positive rate (TPR) that was 3.9 and 10.4 times higher than 'background network' and 'phosphorylation only' approaches, respectively (Figure S7B). Thus, our network-based approach correctly identified known signaling-to-transcription relationships between canonical TLR pathway components thanks to the information collected using DCs in this study.

Next, we searched for biochemical paths connecting the 29 signaling regulators highlighted above as 'seeds' (Figure 5A), and the 782 TFs detected by mass spectrometry in BMDCs as 'targets' (Table S1). We identified 420 significant relationships between 27/29 'seed' (except for seed DMXL2 and RAB3IL1) and 95/782 'target' nodes ($p < 0.0005$, FDR < 0.05), whereas only 12 relationships linking 7 'seeds' to 11 'targets' can be found without integrating our DC-specific data sets with publicly available interactions within our algorithmic framework (Figure 7B and Table S7). Each signaling node reached between 51 (TBK1) and 3 (ARHGEF11) TFs, for an average of 14.5 +/− 11.6 S.D. TFs via 1.5 +/− 0.7 S.D. intermediate nodes (Figure S7C). Importantly, these signaling-to-transcription relationships captured 11 out of the 14 canonical TLR TFs, and to 8/20 of the TFs whose binding sites were compared to knockdown effects (Figure 5B, 7C and 7D). Furthermore, 49% (47/95) of the TFs were both up-regulated at the phosphorylation level upon LPS

stimulation and downregulated in *Myd88*$^{-/-}$/*Ticam1*$^{-/-}$ cells. Overall, each of the three modules identified based on co-phenotypes upon knockdown (Figure 5), appeared to be biochemically linked to similar downstream TFs (Figure 7D).

We asked which intermediate nodes were most central between seed and target nodes (*i.e.*, most connected to target TF nodes). For the 420 significant relationships linking the 27 seed and 95 target nodes, we ranked the top 25 intermediates present across each of our three modules (Figure 7D), which lead to a total of 60 non-overlapping intermediate nodes that included 16 canonical TLR pathway components (Figure 7E, 7F). These 60 intermediate nodes displayed various levels of specificity across the 3 modules identified above, with for example IRAK4 being central to module II (*i.e.*, connected to a relatively high number of nodes), whereas MAPK8 (JNK) and MAPK14 (P38) were more connected across modules I and III, respectively. Other nodes appeared shared between modules such as AKT1 for I and III, or TAB2 for I, II and III. Thus, intermediate nodes display both specific and shared roles across the regulatory modules of the TLR4 pathway, which likely reflects crosstalk within pathways leading to the regulation of overlapping sets of target genes.

To gain insights into how signal is distributed downstream of TLR4, we asked how the 420 seed-target relationships identified here were affected by the 4 knockout strains used in this study (Figure 6D). We quantified how many of the nodes (seed, intermediate, and target) present in each of the 420 seed-target pairs were impacted at their phosphorylation level by knockout. 391 out of the 420 pairs were significantly affected by *Myd88*$^{-/-}$/*Ticam1*$^{-/-}$, and 261 out of these 391 pairs were also impacted by *Myd88*$^{-/-}$, *Irak2*$^{-/-}$, and/or *Irak4*$^{-/-}$, leading to four clusters of effects: (i) double KO only or together with (ii) IRAK4 alone, (iii) IRAK4 and MYD88, (iv) IRAK4, MYD88 and IRAK2 (although to a lesser extent) (Figure 7G). Interestingly, a large fraction of TLR4 signals were impacted by MYD88 deletion, as expected, but IRAK4 was responsible for broader effects despite the presence of IRAK4 and MYD88 in the same complex. Seed-target pairs that were impacted only by double KO cells but not MYD88 KO are likely to be important for TRIF-dependent signaling (*i.e.*, module II). Overall, this quantitative measurement of KO effects on signaling-to-transcription paths provides additional information on how signal is transmitted and partitioned from MYD88 and some of its kinase partners to downstream signaling and transcriptional regulatory layers.

Discussion

We established an integrative framework to dissect signal propagation in the TLR system using data spanning both signaling and transcriptional regulatory events. Previous studies have connected paths within networks largely using protein-protein interaction or phosphorylation data alone, or in conjunction with one to two different types of experimental data (Gitter et al., 2013; Huang and Fraenkel, 2009; Huang et al., 2013; Terfve et al., 2015). This study provides a proof-of-principle example of the power of integrative analyses that take into account regulatory layers not typically studied in conjunction – from phosphorylation dynamics, to relationships between kinases substrates, to proteins forming complexes or binding to DNA, to gene regulation. In future work, it will be crucial to take into account additional regulatory layers such as the spatial distribution of proteins

(Brubaker et al., 2015), other post-translational modifications and their enzymes (*e.g.*, ubiquitination, acetylation) (Mertins et al., 2013), and post-transcriptional modifications (RNA) or translational control events.

The observations that AP1AR, its binding partner PICALM, and SAMHD1 might play a role in pro-inflammatory signaling will require future mechanistic studies. Interestingly, both AP1AR and its binding partner PICALM interact with clathrin adaptor proteins (Maritzen and Haucke, 2010; Miller et al., 2015), suggesting a link between the TLR4-MYD88 pathway and intracellular vesicle transport regulation that is reminiscent of the TLR4-TRIF axis (Kagan et al., 2008). In addition, previous work linked the *Ap1ar* locus to TNF production by DCs triggering colitis (Ermann et al., 2011), which further support our results on the role of AP1AR in pro-inflammatory signaling. The other candidate regulator reported here, SAMHD1, is best characterized in viral restriction (Ballana and Esté, 2015), but also plays a role in processes such as TNF-mediated pro-inflammatory signaling in fibroblasts (Liao et al., 2008), cell cycle (Pauls et al., 2014), or DNA damage (Clifford et al., 2014), and in disease such as the Aicardi– Goutières syndrome (Crow and Manel, 2015), and cancer (Schuh et al., 2012). LPS regulated both known and previously unrecognized phosphosites on SAMHD1 such as T634, mouse orthologue site for the known human T592 regulatory site targeted by CDK2 (Pauls et al., 2014), or T52 found in the poorly characterized SAM domain and that was regulated in a MYD88-dependent manner. Taken together, these observations provide valuable information for future mechanistic investigations.

The multi-layer data sets reported here will be useful for further analyses, mining and hypothesis-generating purposes on additional candidate regulators – from the protein to the phosphosite level. First, many of the 131 phosphoproteins selected for genetic screening had little to no effects on gene expression. While poor knockdown efficiency and functional redundancy can likely explain some of these cases, measuring the effects of perturbing these proteins on other aspects of DC biology such as motility or antigen presentation might help uncover important mechanisms. Second, we focused our targeted screen for regulators of gene expression on enzymes and their regulators, but screening additional molecular functions is likely to uncover additional regulators. For example, 24 phosphoproteins down-regulated between 180 and 240 min after LPS stimulation are involved in RNA binding and include known pathogen-sensing regulators *Ddx21*, *Ddx3x*, or *Adar* and a host of potential candidates for this nascent area in TLR biology (Anderson, 2010).

Lastly, it will be critical to build upon this work to systematically identify functional phosphosites and their matching kinases. Our study correctly identified many phosphosites of canonical TLR components or other pathogen-sensing pathways such as NLRC4 S533, which is a key site for host immunity (Qu et al., 2012). Our large-scale *in vitro* kinase assay uncovered many known and candidate substrates which will be important to validate using *in vivo* chemical genetics approaches (Allen et al., 2007), and shorter timescales to increase confidence about substrate specificity as shown in bacteria and yeast (Kanshin et al., 2015; Skerker et al., 2008). Thus, future research on screening functional phosphosites using site-directed mutagenesis will help to reveal phosphorylated residues with functional significance and potential therapeutic value.

Experimental Procedures

Cells

Bone marrow-derived DCs were generated from 6–8 week old female C57BL/6J (Jackson Laboratories), *Ap1ar*$^{-/-}$ (Maritzen et al., 2012), *Samhd1*$^{-/-}$ (Rehwinkel et al., 2013), *Myd88*$^{-/-}$, *Myd88*$^{-/-}$/*Ticam*$^{-/-}$, *Irak2*$^{-/-}$, *Irak4*$^{-/-}$ mice. All stimulations were performed using ultra-pure *E. coli* K12 LPS (Invivogen) at 100 ng/mL. For shRNA knockdowns, high-titer lentiviruses expressing shRNAs were used to infect bone marrow cells as previously described (Chevrier et al., 2011).

mRNA measurements

Total or poly(A)$^+$ RNA was extracted and reverse transcribed prior to qPCR analysis with SYBR Green (Roche) in triplicate with *Gapdh* for normalization. For mRNA counting, 5×10^4 bone marrow-derived DCs were lysed in RLT buffer (Qiagen) with 1% β-ME. 10% of the lysate was used for mRNA counting using the nCounter Digital Analyzer (NanoString) and a custom CodeSet constructed to detect a total of 267 genes (including 16 control genes whose expression remain unaffected by TLR stimulation). To determine significantly affected signature genes, a fold-change ratio is computed for each pairwise comparison of a knockdown sample versus a set of control samples (*i.e.*, non-targeting shRNA; at least 10 per experimental batch).

Affinity purification followed by mass spectrometry

Analysis of interaction partners of V5-tagged proteins (MYD88, IRAK2 and AP1AR) was performed using a single-step purification procedure as previously described (Hubner and Mann, 2011), with several modifications. Peptide samples were analyzed on a Q Exactive mass spectrometer (Thermo Fisher Scientific), and mass spectra processed as described above.

Large-scale phosphoproteome and proteome analyses

For temporal phosphoproteome analysis, BMDCs grown in SILAC media were stimulated with LPS, and lysed and processed for enrichment of phosphopeptides using SCX/IMAC as described previously (Chevrier et al., 2011; Mertins et al., 2013). For *in vitro* kinase (IVK) and knockout (KO) phosphoproteome analysis, peptide samples were separated by basic reversed-phase (RP) prior to IMAC enrichment as described previously (Mertins et al., 2013). *In vitro* kinase reactions were performed with recombinant kinases for IRAK2, IRAK4 or TBK1 on SILAC-labeled native cell lysates from DCs. For proteome analysis, total peptides were separated into 12 fractions using an Agilent 3100 Offgel fractionator. Peptide samples were analyzed on LTQ Orbitrap, LTQ Orbitrap Velos or Q Exactive mass spectrometer (Thermo Fisher Scientific). To identify and quantify peptides, mass spectra were processed with the Spectrum Mill (Agilent Technologies) and the MaxQuant (version 1.2.2.5) software packages (Cox and Mann, 2008). Details on differential expression, clustering, pathway enrichment, and network analyses are in the Supplemental Experimental Procedures.

Supplementary Material

Refer to Web version on PubMed Central for supplementary material.

Acknowledgments

We thank Diane Mathis, Laurie Glimcher, Paul Anderson, Mikael Pittet, Jeroen Saeij, Jonathan Kagan, Ido Amit, D.R. Mani and members of the Hacohen, Regev, and Carr laboratories for helpful discussions. We are grateful to Yanick Crow and Gillian Rice for human fibroblast cell lines from Aicardi–Goutières syndrome patients, and to Jan Rehwinkel for *Samhd1*$^{-/-}$ mouse bone marrow cells.

References

Allen JJ, Li M, Brinkworth CS, Paulson JL, Wang D, Hübner A, Chou W-H, Davis RJ, Burlingame AL, Messing RO, et al. A semisynthetic epitope for kinase substrates. Nat Meth. 2007; 4:511–516.

Anderson P. Post-transcriptional regulons coordinate the initiation and resolution of inflammation. Nature Reviews Immunology. 2010; 10:24–35.

Ballana E, Esté JA. SAMHD1: At the Crossroads of Cell Proliferation, Immune Responses, and Virus Restriction. Trends in Microbiology. 2015; 23:680–692. [PubMed: 26439297]

Bensimon A, Heck AJR, Aebersold R. Mass spectrometry-based proteomics and network biology. Annu. Rev. Biochem. 2012; 81:379–405. [PubMed: 22439968]

Bodenmiller B, Wanka S, Kraft C, Urban J, Campbell D, Pedrioli PG, Gerrits B, Picotti P, Lam H, Vitek O, et al. Phosphoproteomic analysis reveals interconnected system-wide responses to perturbations of kinases and phosphatases in yeast. Science Signaling. 2010; 3:rs4–rs4. [PubMed: 21177495]

Brubaker SW, Bonham KS, Zanoni I, Kagan JC. Innate immune pattern recognition: a cell biological perspective. Annu. Rev. Immunol. 2015; 33:257–290. [PubMed: 25581309]

Chevrier N, Mertins P, Artyomov MN, Shalek AK, Iannacone M, Ciaccio MF, Gat-Viks I, Tonti E, DeGrace MM, Clauser KR, et al. Systematic discovery of TLR signaling components delineates viral-sensing circuits. Cell. 2011; 147:853–867. [PubMed: 22078882]

Clifford R, Louis T, Robbe P, Ackroyd S, Burns A, Timbs AT, Wright Colopy G, Dreau H, Sigaux F, Judde JG, et al. SAMHD1 is mutated recurrently in chronic lymphocytic leukemia and is involved in response to DNA damage. Blood. 2014; 123:1021–1031. [PubMed: 24335234]

Cox J, Mann M. MaxQuant enables high peptide identification rates, individualized p.p.b.-range mass accuracies and proteome-wide protein quantification. Nature Biotechnology. 2008; 26:1367–1372.

Crow YJ, Manel N. Aicardi-Goutières syndrome and the type I interferonopathies. Nature Reviews Immunology. 2015; 15:429–440.

Eriksen AB, Torgersen ML, Holm KL, Abrahamsen G, Spurkland A, Moskaug JØ, Simonsen A, Blomhoff HK. Retinoic acid-induced IgG production in TLR-activated human primary B cells involves ULK1-mediated autophagy. Autophagy. 2015; 11:460–471. [PubMed: 25749095]

Ermann J, Garrett WS, Kuchroo J, Rourida K, Glickman JN, Bleich A, Glimcher LH. Severity of innate immune-mediated colitis is controlled by the cytokine deficiency-induced colitis susceptibility-1 (Cdcs1) locus. Proc. Natl. Acad. Sci. U.S.a. 2011; 108:7137–7141. [PubMed: 21482794]

Garber M, Yosef N, Goren A, Raychowdhury R, Thielke A, Guttman M, Robinson J, Minie B, Chevrier N, Itzhaki Z, et al. A high-throughput chromatin immunoprecipitation approach reveals principles of dynamic gene regulation in mammals. Molecular Cell. 2012; 47:810–822. [PubMed: 22940246]

Geng J, Sun X, Wang P, Zhang S, Wang X, Wu H, Hong L, Xie C, Li X, Zhao H, et al. Kinases Mst1 and Mst2 positively regulate phagocytic induction of reactive oxygen species and bactericidal activity. Nat Immunol. 2015; 16:1142–1152. [PubMed: 26414765]

Gitter A, Carmi M, Barkai N, Bar-Joseph Z. Linking the signaling cascades and dynamic regulatory networks controlling stress responses. Genome Research. 2013; 23:365–376. [PubMed: 23064748]

Hasan UA, Caux C, Perrot I, Doffin A-C, Menetrier-Caux C, Trinchieri G, Tommasino M, Vlach J. Cell proliferation and survival induced by Toll-like receptors is antagonized by type I IFNs. Proceedings of the National Academy of Sciences. 2007; 104:8047–8052.

Huang S-SC, Fraenkel E. Integrating proteomic, transcriptional, and interactome data reveals hidden components of signaling and regulatory networks. Science Signaling. 2009; 2:ra40–ra40. [PubMed: 19638617]

Huang S-SC, Clarke DC, Gosline SJC, Labadorf A, Chouinard CR, Gordon W, Lauffenburger DA, Fraenkel E. Linking proteomic and transcriptional data through the interactome and epigenome reveals a map of oncogene-induced signaling. PLoS Comput Biol. 2013; 9:e1002887. [PubMed: 23408876]

Hubner NC, Mann M. Extracting gene function from protein-protein interactions using Quantitative BAC InteraCtomics (QUBIC). Methods. 2011; 53:453–459. [PubMed: 21184827]

Huttlin EL, Ting L, Bruckner RJ, Gebreab F, Gygi MP, Szpyt J, Tam S, Zarraga G, Colby G, Baltier K, et al. The BioPlex Network: A Systematic Exploration of the Human Interactome. Cell. 2015; 162:425–440. [PubMed: 26186194]

Kagan JC, Su T, Horng T, Chow A, Akira S, Medzhitov R. TRAM couples endocytosis of Toll-like receptor 4 to the induction of interferon-beta. Nature Medicine. 2008; 9:361–368.

Kanshin E, Bergeron-Sandoval L-P, Isik SS, Thibault P, Michnick SW. A cell-signaling network temporally resolves specific versus promiscuous phosphorylation. CellReports. 2015; 10:1202–1214.

Kawagoe T, Sato S, Matsushita K, Kato H, Matsui K, Kumagai Y, Saitoh T, Kawai T, Takeuchi O, Akira S. Sequential control of Toll-like receptor-dependent responses by IRAK1 and IRAK2. Nat Immunol. 2008; 9:684–691. [PubMed: 18438411]

Li S, Wang L, Berman M, Kong Y-Y, Dorf ME. Mapping a dynamic innate immunity protein interaction network regulating type I interferon production. Immunity. 2011; 35:426–440. [PubMed: 21903422]

Liao W, Bao Z, Cheng C, Mok Y-K, Wong WSF. Dendritic cell-derived interferon-γ-induced protein mediates tumor necrosis factor-α stimulation of human lung fibroblasts. Proteomics. 2008; 8:2640–2650. [PubMed: 18546154]

Maritzen T, Haucke V. Gadkin: A novel link between endosomal vesicles and microtubule tracks. Commun Integr Biol. 2010; 3:299–302. [PubMed: 20798811]

Maritzen T, Zech T, Schmidt MR, Krause E, Machesky LM, Haucke V. Gadkin negatively regulates cell spreading and motility via sequestration of the actin-nucleating ARP2/3 complex. Proceedings of the National Academy of Sciences. 2012; 109:10382–10387.

Mertins P, Qiao JW, Patel J, Udeshi ND, Clauser KR, Mani DR, Burgess MW, Gillette MA, Jaffe JD, Carr SA. Integrated proteomic analysis of post-translational modifications by serial enrichment. Nat Meth. 2013; 10:634–637.

Miller SE, Mathiasen S, Bright NA, Pierre F, Kelly BT, Kladt N, Schauss A, Merrifield CJ, Stamou D, Höning S, et al. CALM regulates clathrin-coated vesicle size and maturation by directly sensing and driving membrane curvature. Developmental Cell. 2015; 33:163–175. [PubMed: 25898166]

Pauls E, Ruiz A, Badia R, Permanyer M, Gubern A, Riveira-Muñoz E, Torres-Torronteras J, Álvarez M, Mothe B, Brander C, et al. Cell Cycle Control and HIV-1 Susceptibility Are Linked by CDK6-Dependent CDK2 Phosphorylation of SAMHD1 in Myeloid and Lymphoid Cells. The Journal of Immunology. 2014; 193:1988–1997. [PubMed: 25015816]

Picard C, Puel A, Bonnet M, Ku C-L, Bustamante J, Yang K, Soudais C, Dupuis S, Feinberg J, Fieschi C, et al. Pyogenic bacterial infections in humans with IRAK-4 deficiency. Science. 2003; 299:2076–2079. [PubMed: 12637671]

Qu Y, Misaghi S, Izrael-Tomasevic A, Newton K, Gilmour LL, Lamkanfi M, Louie S, Kayagaki N, Liu J, Kömüves L, et al. Phosphorylation of NLRC4 is critical for inflammasome activation. Nature. 2012; 490:539–542. [PubMed: 22885697]

Rehwinkel J, Maelfait J, Bridgeman A, Rigby R, Hayward B, Liberatore RA, Bieniasz PD, Towers GJ, Moita LF, Crow YJ, et al. SAMHD1-dependent retroviral control and escape in mice. The EMBO Journal. 2013; 32:2454–2462. [PubMed: 23872947]

Sanada T, Takaesu G, Mashima R, Yoshida R, Kobayashi T, Yoshimura A. FLN29 deficiency reveals its negative regulatory role in the Toll-like receptor (TLR) and retinoic acid-inducible gene I (RIG-I)-like helicase signaling pathway. J. Biol. Chem. 2008; 283:33858–33864. [PubMed: 18849341]

Santra T, Kolch W, Kholodenko BN. Navigating the multilayered organization of eukaryotic signaling: a new trend in data integration. PLoS Comput Biol. 2014; 10:e1003385. [PubMed: 24550716]

Schuh A, Becq J, Humphray S, Alexa A, Burns A, Clifford R, Feller SM, Grocock R, Henderson S, Khrebtukova I, et al. Monitoring chronic lymphocytic leukemia progression by whole genome sequencing reveals heterogeneous clonal evolution patterns. Blood. 2012; 120:4191–4196. [PubMed: 22915640]

Sharma K, Kumar C, Kéri G, Breitkopf SB, Oppermann FS, Daub H. Quantitative analysis of kinase-proximal signaling in lipopolysaccharide-induced innate immune response. J. Proteome Res. 2010; 9:2539–2549. [PubMed: 20222745]

Sjoelund V, Smelkinson M, Nita-Lazar A. Phosphoproteome profiling of the macrophage response to different toll-like receptor ligands identifies differences in global phosphorylation dynamics. J. Proteome Res. 2014; 13:5185–5197. [PubMed: 24941444]

Skerker JM, Perchuk BS, Siryaporn A, Lubin EA, Ashenberg O, Goulian M, Laub MT. Rewiring the specificity of two-component signal transduction systems. Cell. 2008; 133:1043–1054. [PubMed: 18555780]

Suzuki N, Suzuki S, Duncan GS, Millar DG, Wada T, Mirtsos C, Takada H, Wakeham A, Itie A, Li S, et al. Severe impairment of interleukin-1 and Toll-like receptor signalling in mice lacking IRAK-4. Nature. 2002; 416:750–756. [PubMed: 11923871]

Takeuchi O, Akira S. Pattern recognition receptors and inflammation. Cell. 2010; 140:805–820. [PubMed: 20303872]

Tanigawa K, Suzuki K, Kimura H, Takeshita F, Wu H, Akama T, Kawashima A, Ishii N. Tryptophan aspartate-containing coat protein (CORO1A) suppresses Toll-like receptor signalling in Mycobacterium leprae infection. Clin. Exp. Immunol. 2009; 156:495–501. [PubMed: 19438603]

Terfve CDA, Wilkes EH, Casado P, Cutillas PR, Saez-Rodriguez J. Large-scale models of signal propagation in human cells derived from discovery phosphoproteomic data. Nature Communications. 2015; 6:8033.

Weintz G, Olsen JV, Frühauf K, Niedzielska M, Amit I, Jantsch J, Mages J, Frech C, Dölken L, Mann M, et al. The phosphoproteome of toll-like receptor-activated macrophages. Molecular Systems Biology. 2010; 6:371. [PubMed: 20531401]

Yugi K, Kubota H, Hatano A, Kuroda S. Trans-Omics: How To Reconstruct Biochemical Networks Across Multiple “Omic” Layers. Trends in Biotechnology. 2016; 34:276–290. [PubMed: 26806111]

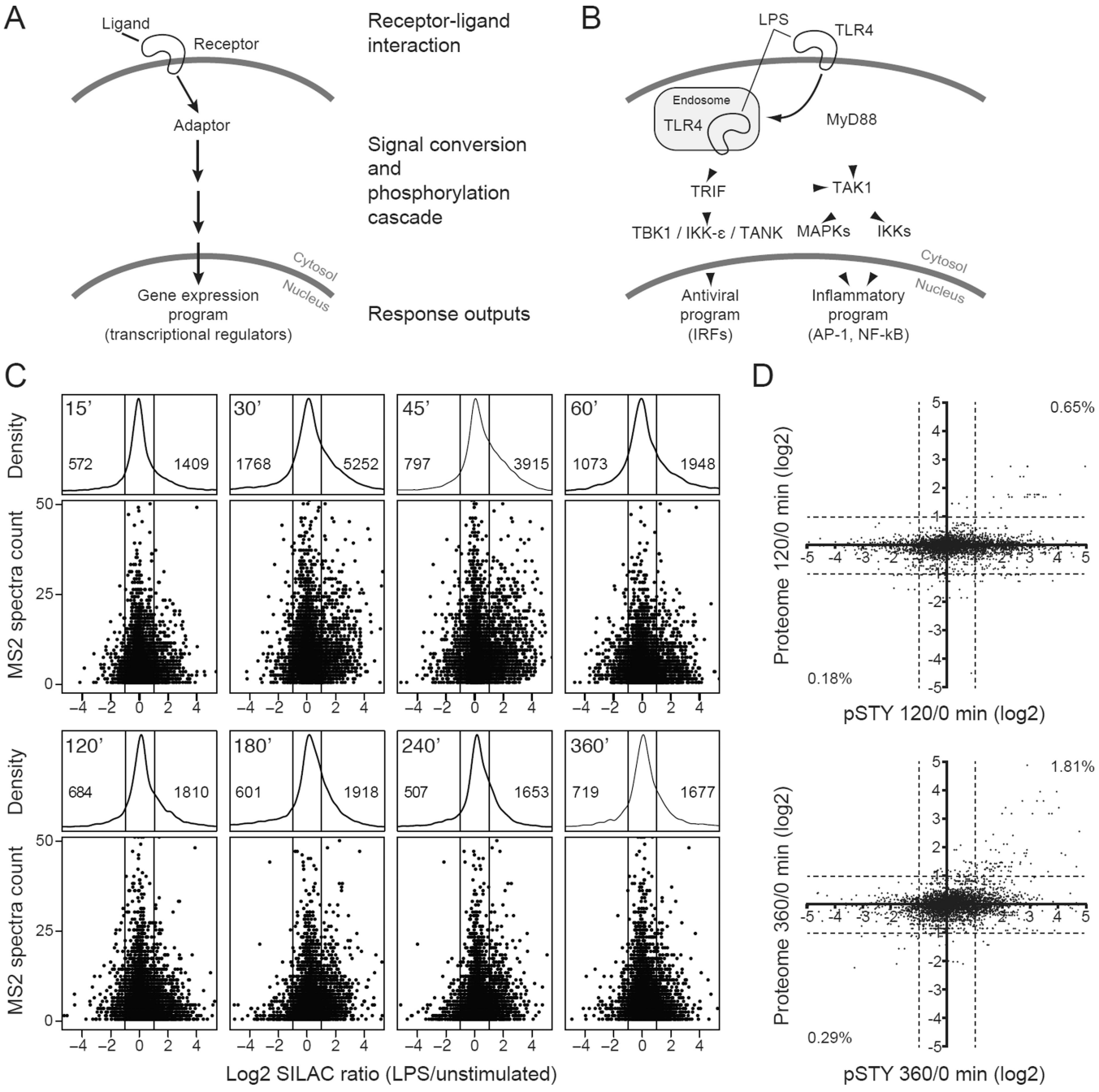

Figure 1. TLR4 stimulation with LPS leads to global and dynamic changes in the phosphoproteome of dendritic cells (DCs)

(A–B) Diagram highlighting general principles of cellular signaling-to-transcription events (A) and their transposition to the TLR4 pathway (B).

(C) Temporal changes in the phosphoproteome of LPS-stimulated DCs. Shown are the distributions of log2 fold changes of phosphosites (X axis) between LPS-treated and untreated cells at indicated times after LPS stimulation, as density (top of each panel) and dot plots (bottom of each panel, with MS2 spectra count in Y axis and showing phosphosites measured in all 8 time points).

(D) Comparison between the phosphoproteome and total proteome of LPS-stimulated DCs. Shown are distributions of log2 fold changes of phosphosites (X axis) and proteins (Y axis) between LPS-treated and untreated cells at 120 (top) and 360 (bottom) min post-stimulation. See also Figure S1 and Table S1.

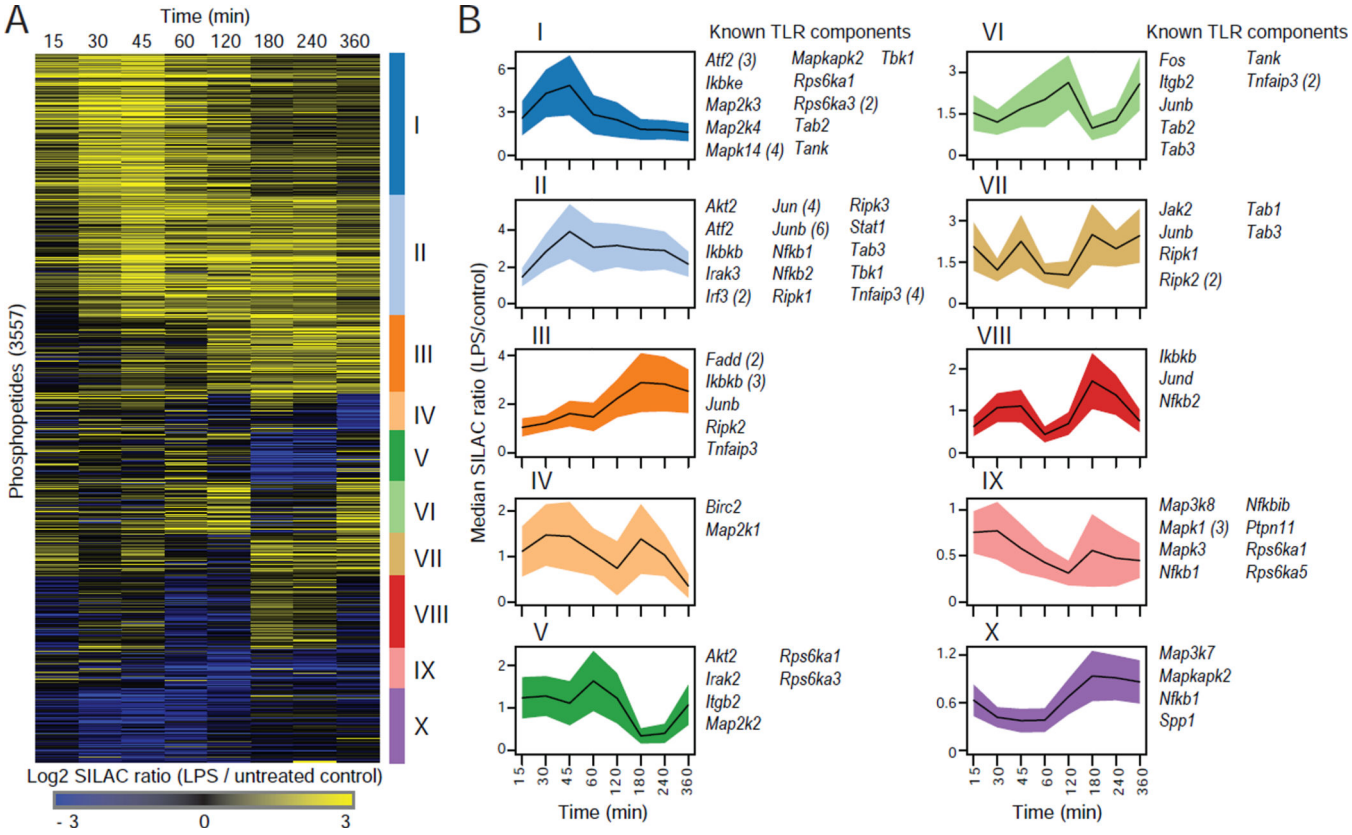

Figure 2. Temporal analysis of the LPS-induced phosphoproteome reveals known and candidate regulators of TLR4 signaling

(A) Temporal phosphorylation profiles during LPS stimulation in DCs. Log2 fold changes between LPS-treated and untreated cells for 3557 phosphosites (rows) detected in at least 6 out of 8 time points (columns). Phosphosites are partitioned into 10 clusters using k-means (color bars, right). White indicates missing values.

(B) Median log2 fold changes between LPS-treated and untreated cells (y axis) and median absolute deviation (MAD, colored error bar) at each time point (x axis) for phosphosites in all 10 k-means clusters from A. Known TLR pathway proteins detected in each cluster are indicated on the right. Parentheses indicate the number of phosphosites per proteins (when > 1).

See also Figure S2 and Table S2.

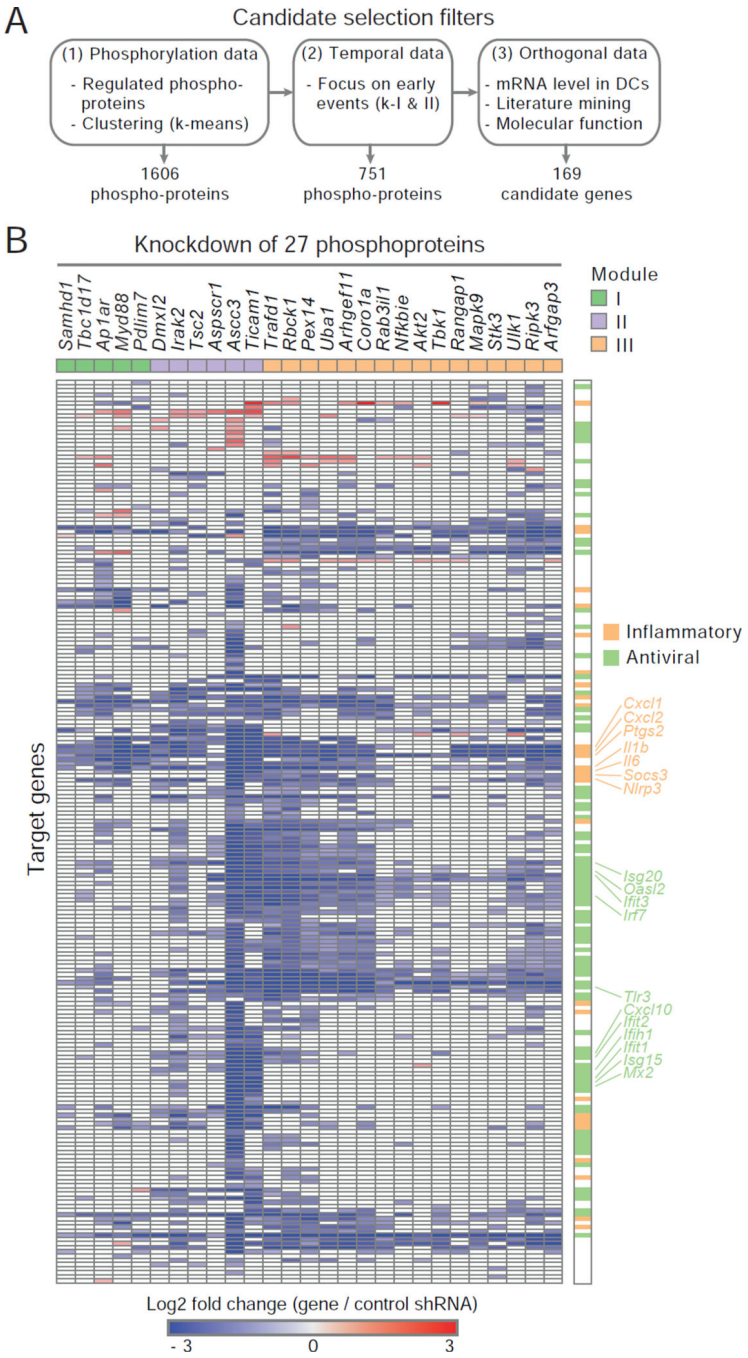

Figure 3. Genetic perturbations of phosphorylated proteins identify putative regulators of TLR4 signaling

(A) Overview of phosphoprotein candidate selection for functional analysis.

(B) Perturbation profiles of the 27 phosphoproteins that significantly impacted TLR4 outputs. Shown are the perturbed candidates and control phosphoproteins (columns) and the log2 fold changes for each target gene (rows) between gene-specific and control shRNAs. The right-most column categorizes target genes into antiviral (light green) and inflammatory (light orange) programs.

See also Figure S3 and Table S3.

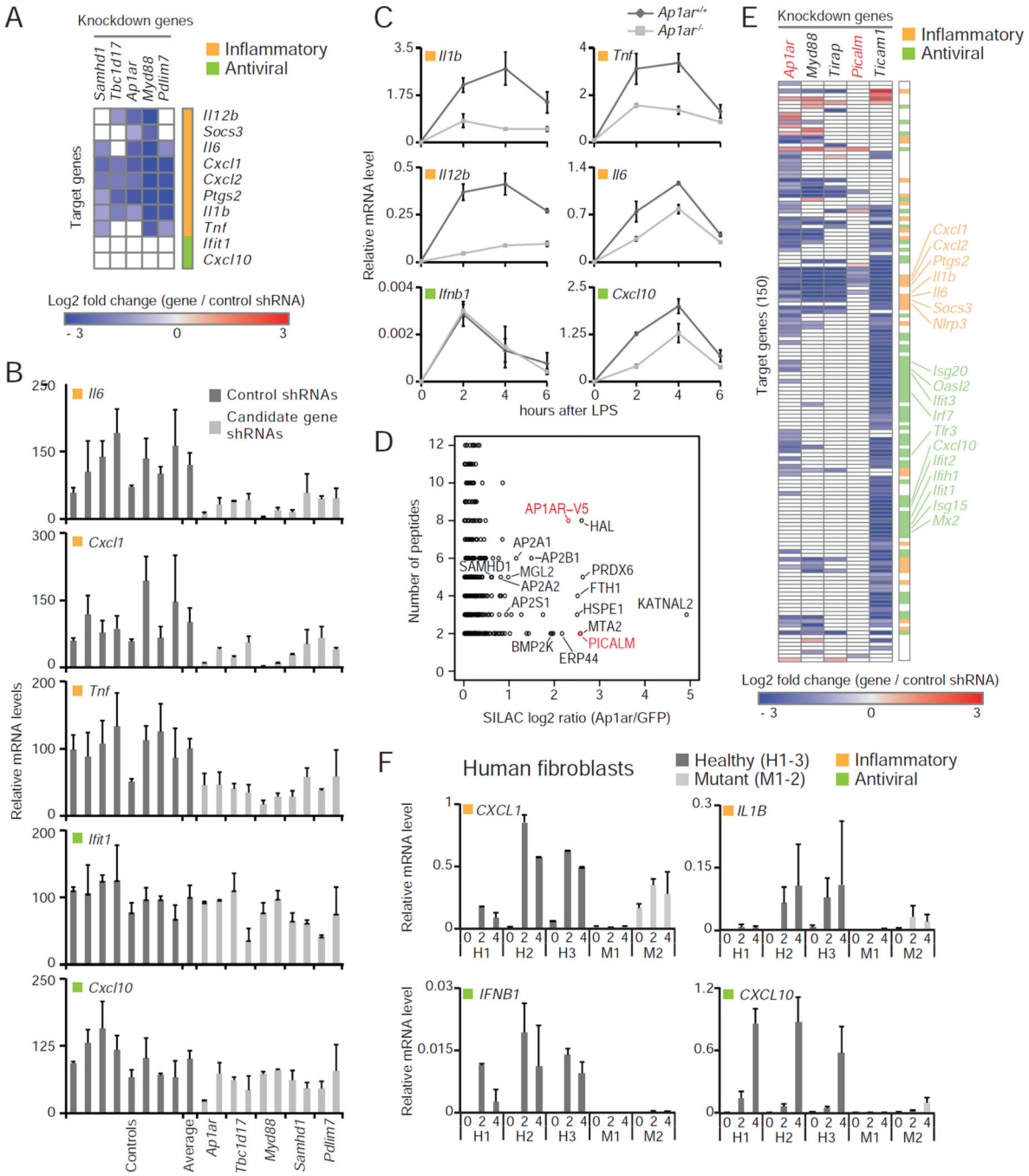

Figure 4. Identification of candidate regulators in the MYD88-dependent inflammatory pathway

(A) Perturbation profiles of genes affecting the MYD88 pathway. Shown are 4 perturbed candidate genes and MYD88 (columns) and the log2 fold changes between gene-specific and control shRNAs (rows) of 10 target genes. The right-most column categorizes target genes into antiviral (light green) and inflammatory (light orange) programs.

(B) Expression levels (qPCR) relative to control shRNAs (left bars, dark grey) for two antiviral cytokines (*Ifit1* and *Cxcl10*) and for three inflammatory cytokines (*Il6*, *Cxcl1*, and *Tnf*), following LPS stimulation in DCs using two independent shRNAs. Bottom tick marks

separate shRNAs controls and each gene ('Average' indicate the mean value for all 8 control shRNAs). Two to three replicates for each experiment; error bars are the standard deviations.
(C) Inhibition of transcription of inflammation cytokines in *Ap1ar*$^{-/-}$ DCs. mRNA levels (qPCR; relative to Gapdh) for indicated inflammatory (light orange) and antiviral (light green) cytokines in three replicates per time point. Error bars represent the standard deviation.
(D) Interaction proteomics identified putative binders for AP1AR in DCs. Log2 fold change (X axis) of proteins identified between DCs expressing V5-tagged-AP1AR and -GFP (control bait) plotted against the number of peptides identified per protein (Y axis).
(E) Perturbation profiles of indicated genes (columns) and the log2 fold changes between gene-specific and control shRNAs (rows) of 150 target genes. The right-most column categorizes target genes into antiviral (light green) and inflammatory (light orange) programs.
(F) Impact of SAMHD1 mutations on human fibroblast cell response to LPS. Human fibroblasts from healthy (H) or mutant-carrying patients (M; with homozygous c.445C>T p.Gln149* for M1 and c.1609-1G>C for M2) were stimulated with LPS or left untreated as control, and indicated inflammatory (light orange) and antiviral (light green) cytokine levels were measured by qPCR (relative to GAPDH). Error bars represent the standard deviation. See also Figure S4 and Table S4.

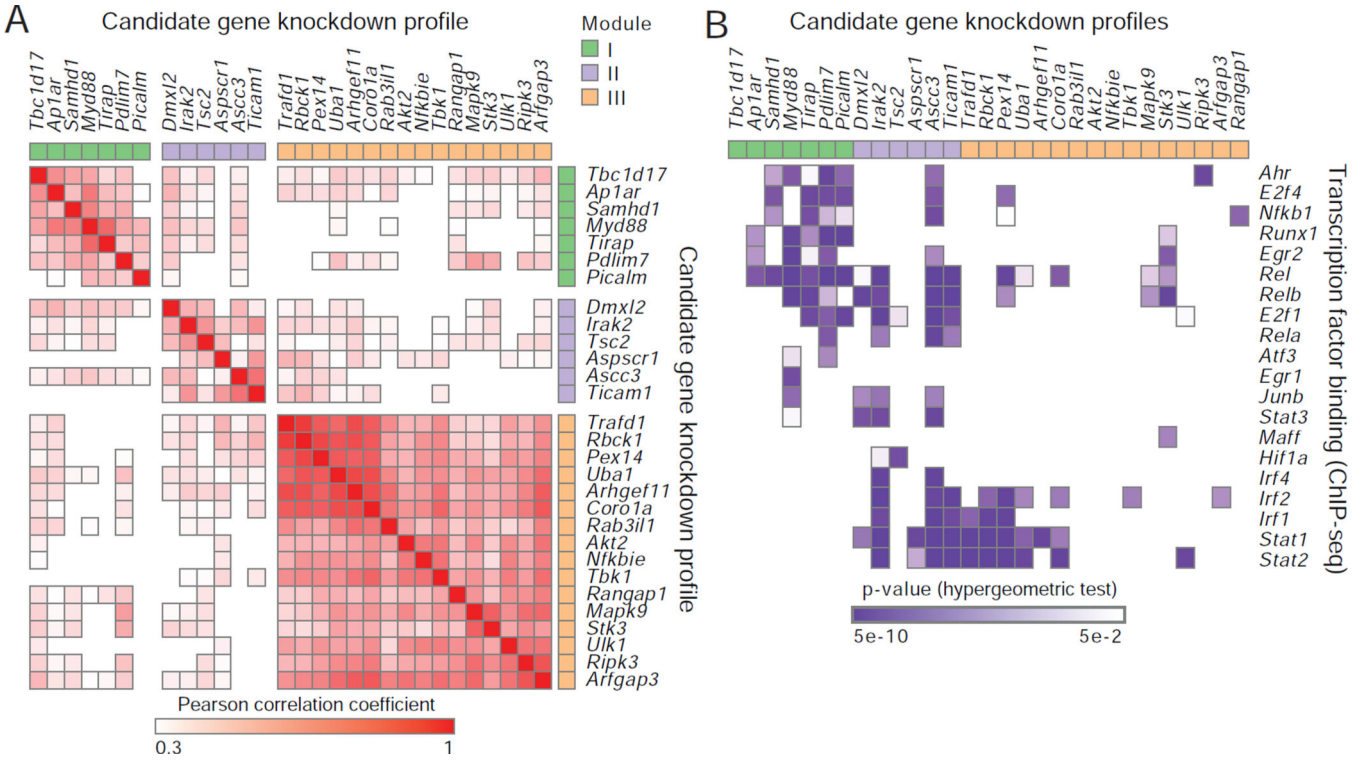

Figure 5. Similarities in perturbation profiles and overlap with transcription factor target genes suggest three functional modules for the 29 candidate phosphoproteins

(A) Functional classification based on similarity of perturbation profiles. Shown is a correlation matrix (Pearson correlation coefficient) of the perturbation profiles from Figures 3B and 4E combined.

(B) Intersection between genes affected by a phosphoprotein perturbation and genes whose promoters are bound by transcription factors (TFs). Shown are the overlaps between genes affected by 29 candidate signaling regulators knockdowns (columns, including positive control genes) and genes whose promoters are bound by 20 TFs (rows). P values, hypergeometric test (purple: significant correlation; white: no correlation).

See also Figure S5 and Table S5.

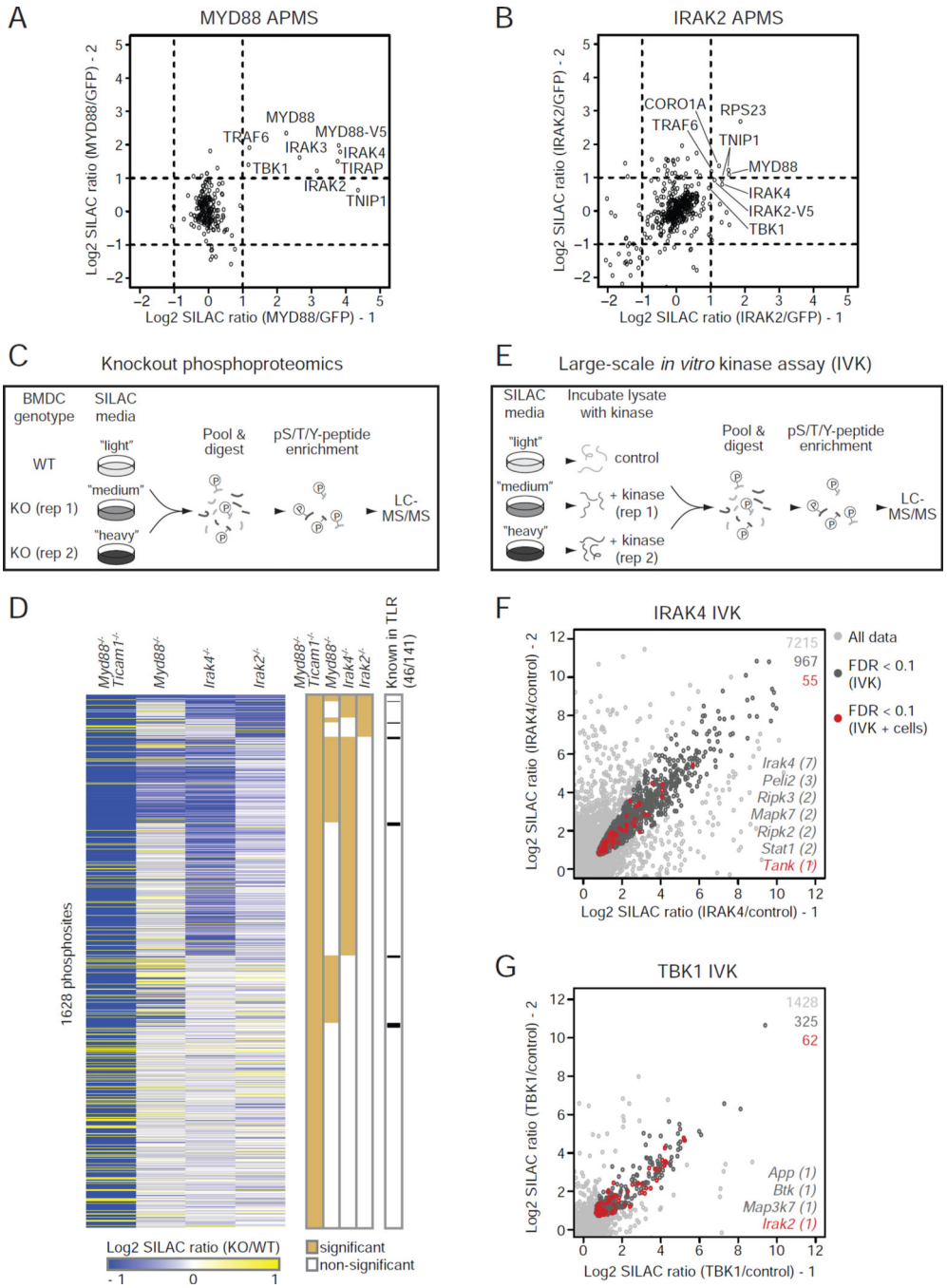

Figure 6. Physical and functional proteomics assays pinpoint binding and phosphorylation events downstream of the Myd88 adaptor and associated kinases

(A–B) Affinity purification followed by proteomics. Shown are dot plots of SILAC ratios for proteins identified in DCs overexpressing V5-tagged MYD88 (A) or IRAK2 (B). Cells were stimulated with LPS for 30 min, and protein complexes purified using anti-V5 antibodies coupled to magnetic beads. Each axis represents an independent experiment.

(C) Diagram depicting our experimental approach for measuring the impact of gene knockout on the TLR4-regulated phosphoproteome of mouse BMDCs.

(D) Phosphoproteomics in KO cells. Left, shown is a heatmap for SILAC ratios of phosphosites (rows) in 4 KO models (columns) at 30 min after LPS stimulation compared to control wild-type cells, as indicated (grey, missing values). Middle, shown in light brown are phosphosites with significant up- or down-regulation in KO vs WT. Right, shown in black are the phosphosites belonging to known TLR proteins.
(E) Diagram depicting our experimental approach for large-scale in vitro kinase assays using native protein lysates from BMDCs and phosphoproteomics.
(F–G) In vitro kinase (IVK) assay followed by phosphoproteomics. Shown are scatter plots of SILAC ratios of phosphosites identified using purified kinases: IRAK4 (D) and TBK1 (E). Light grey, all data points; dark grey, phosphosites with FDR < 0.1 in IVK; red, phosphosites with FDR < 0.1 in both IVK and in cells stimulated with LPS, which highlights the overlap between IVK and phosphoproteome measurements on stimulated cells (denoted as IVK + cells). Gene names at the bottom right of each plot indicate known TLR components with the number of phosphosites in parenthesis.
See also Figure S6 and Table S6.

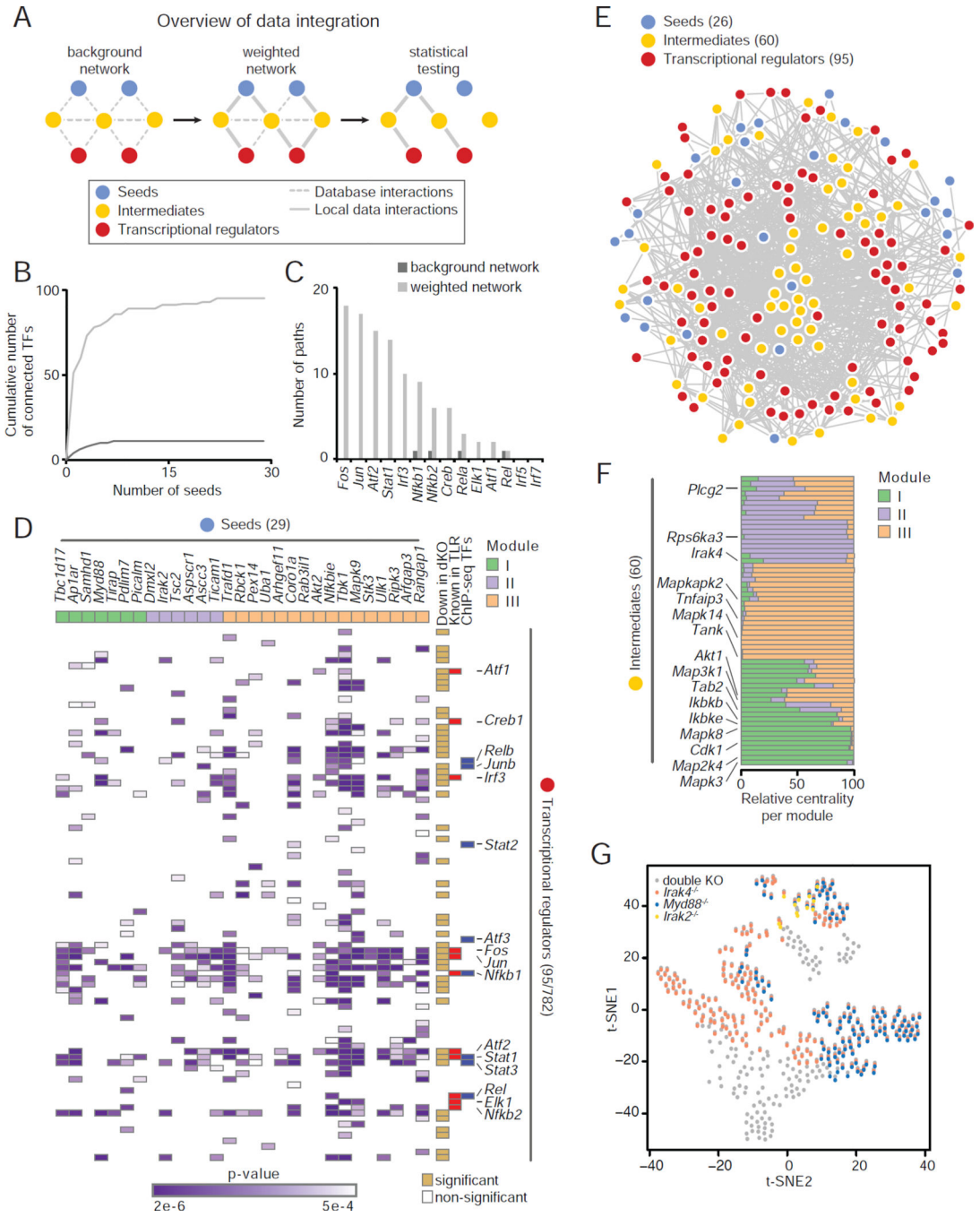

Figure 7. An integrative analysis reveals known and candidate signaling-to-transcription paths and helps parse the effects of Myd88 and associated kinases in the TLR4 system

(A) A computational framework for integrative analysis of the functional and physical proteomics datasets collected in this study (from left to right): a background interaction network is assembled using database and local data, nodes and edges are scored based on experimental evidence from this work, and statistically significant relationships determined by bootstrap analysis.

(B) Cumulative number of significant relationships (boostrap p-value < 0.0005, FDR < 0.05) identified between 'seed nodes' (29) and any of the transcriptional regulators detected in

BMDCs (782 possible ‘target nodes’ in total) using ‘background network’ (dark grey) and ‘weighted network’ (light grey) methods.
(C) Total number of relationships linking seeds (29) and known TLR transcription regulators (14) for ‘background network’ (dark grey) and ‘weighted network’ (light grey) methods.
(D) Significant relationships (420 pairs) found between 29 seeds (columns) and 95 transcriptional regulators (rows). Modules from Figures 3B and 5A are shown (columns) in light green (I), purple (II), and orange (III). Transcriptional regulators with phosphosites with significant up- or down-regulation in *Myd88*$^{-/-}$/*Ticam1*$^{-/-}$ vs WT and in time series are indicated on the right (light brown). P-values, bootstrap (purple).
(E) An interaction network connects 27 seeds (blue) to 95 transcriptional regulators (red) through the top 60 intermediate (yellow) nodes that were ranked based on centrality measure (see Experimental Procedures).
(F) Centrality score of the top 60 intermediate nodes across the three modules from D.
(G) t-distributed stochastic neighbor embedding (t-SNE) analysis of the effects of gene knockout (data from Figure 6D) on the phosphorylation levels of nodes present in the paths mediating the seed-transcriptional regulator relationships identified in panel D. Shown are all of the 391 out of 420 relationships affected by *Myd88*$^{-/-}$/*Ticam1*$^{-/-}$ (grey dots). The effects of Irak4, Myd88 and Irak2 on these paths are overlaid in orange, blue and yellow, respectively.
See also Figure S7 and Table S7.